Electronic Effects of Nitrogen Atoms of Supports on Pt–Ni Rhombic Dodecahedral Nanoframes for Oxygen Reduction

Masaru Kato,[*,†,‡] Ryota Nakahoshiba,[‡] Kazuya Ogura,[‡] Shoichi Tokuda,[‡] Satoshi Yasuda,[#] Kotaro Higashi,[§] Tomoya Uruga,[§,∥] Yohei Uemura,[⊥] Ichizo Yagi*[*,†,‡]

[†]Faculty of Environmental Earth Science and [‡] Graduate School of Environmental Science, Hokkaido University, N10W5, Kita-ku, Sapporo 060-0810, Japan

[#]Research Group for Nanoscale Structure and Function of Advanced Materials, Advanced Science Research Center, Japan Atomic Energy Agency, 2-4 Shirakawa, Tokai, Ibaraki 319-1195, Japan

[§]Innovation Research Center for Fuel Cells, The University of Electro-Communications, Chofugaoka, Chofu, Tokyo 182-8585, Japan.

[∥]Japan Synchrotron Radiation Research Institute, SPring-8, Sayo, Hyogo 679-5198, Japan

[⊥]Laboratory for Environmental Chemistry, Paul Scherrer Institut, OFLB106, PSI, Forschungsstrasse 111, 5232 Villigen, Switzerland

ABSTRACT. Pt-based nanostructures immobilized on carbon supports have been widely used as electrocatalysts. Their catalytic activity can be improved by support modification including nitrogen-doping and coating with nitrogen-containing polymers, where nitrogen atoms possibly interact with surface Pt atoms at the catalyst/support interface. To understand electronic effects of nitrogen-doped and polymer-coated carbon supports on the catalytic activity of Pt-based nanostructured catalysts, we prepared Pt_3Ni nanoframes (NFs) supported on a polybenzimidazole (PBI)-coated and uncoated carbon nanotubes for the oxygen reduction reaction (ORR), and then compared their catalytic activities and electronic properties with those of NFs immobilized on nitrogen-doped and undoped carbon supports. Although both PBI-coating and nitrogen-doping approaches improved the catalytic activity of NFs, *ex situ* X-ray photoelectron spectroscopy and *in situ* X-ray absorption spectroscopy revealed that nitrogen-doping showed electronic effects on NFs whereas PBI-coating showed almost no impact on the electronic state of NFs but stabilized $Pt(OH)_{ad}$ species under electrochemical conditions. Our studies demonstrate that difference in microscopic environments of nitrogen atoms at the catalyst/support interface is highly sensitive to electronic effects of supports on Pt-based electrocatalysts.

INTRODUCTION

Carbon-based support materials have been widely used for Pt and Pt-alloy nanostructured electrocatalysts for various reactions. The catalyst/support interactions play a crucial role in electrocatalytic performance. To improve the electrocatalytic activity and durability, carbon supports can be modified by heteroatom doping.[1-2] For example, nitrogen-doped carbon (NC) supports have been studied to improve the catalytic activity of supported metal nanoparticles for many reactions including nitrobenzene hydrogenation,[3] formic acid oxidation[4] and oxygen reduction reactions (ORR).[5-16]

The ORR is a key reaction in polymer electrolyte fuel cells (PEFCs) and metal–air batteries. The activity of ORR electrocatalysts is known to govern these device performances. In the case of NC supports, nitrogen atoms are doped in graphene sheets and the coordination of these nitrogen atoms to the surface Pt modulates the electronic structure of Pt-based catalysts,[17] leading to the enhancement of the catalytic activity and durability. Nitrogen atoms of NC are also known to interact with ionomers such as Nafion, which work as proton conductors as well as binders between carbon supports, and as a result improve the dispersibility of ionomers on the support.[5]

In addition to the N-doping method, a polymer-coating method with nitrogen-containing polymers has been studied for Pt nanoparticles.[18-21] For example, polybenzimidazole (PBI) can be uniformly and strongly attached to the surface of carbon materials v*ia* π–π interactions and its nitrogen atoms improve the dispersibility as well as catalytic activity of Pt nanoparticles immobilized.[22-24] This PBI-coating method also creates a stable interfacial adhesion with Nafion *via* acid–base interactions, giving homogeneous ionomer distribution on the support.[24-26] This

polymer-coating approach has been applied to simple metal nanoparticles. However, there is a lack of studies for Pt–M alloy (M = Ni, Co, Pd) nanostructured electrocatalysts. Furthermore, both nitrogen-doping and PBI-coating methods could affect electronic interactions at the catalyst/support interface. However, the impact of differences in the electronic interactions on Pt–M alloy nanostructured electrocatalysts remain unclear between these two approaches.

Herein, we investigated catalytic and electronic effects of nitrogen atoms in PBI-coated carbon supports on an ORR Pt–Ni nanostructured electrocatalyst. As the catalyst, we used Pt_3Ni rhombic dodecahedral nanoframes (NFs): Pt_3Ni alloys are known to show relatively high ORR activity in Pt_3M alloys.[27-28] Because the open-framework structure has both the interior and exterior catalytic surfaces for three-dimensional molecular accessibility, Pt_3Ni NFs is known to show high electrocatalytic activity for the ORR in liquid half-cells and fuel cells.[29-31] NFs were deposited on vertically aligned carbon nanotubes (VACNTs) that were coated and uncoated with PBI (NF/PBI/VACNT and NF/VACNT, respectively). Unlike conventional carbon nanotubes, VACNTs have a high specific surface area (800–1000 $m^2\ g^{-1}$) and highly aligned interstitial pores,[32-35] making them ideal carbon supports. To understand the difference of the electronic effects between NF/PBI/VACNT and NF/VACNT, physicochemical measurements including *ex situ* X-ray photoelectron spectroscopy (XPS) and *in situ* Pt L_{III}-edge X-ray absorption spectroscopy (XAS) were performed. After that, these results were compared with results of previously reported NFs supported on NC and a carbon black of Vulcan XC-72 (NF/NC and NF/C, respectively)[8] to understand differences between N-doping and polymer coating approaches and thier electronic effect on NFs.

EXPERIMENTAL SECTION

Materials. Ethanol, hexane, 2-propanol, perchloric acid, oleylamine, acetic acid, toluene, N,N-dimethylacetamide (DMAc), $Ni(NO_3)_2 \cdot 6H_2O$, melamine and 5% Nafion DE520 were purchased from Wako Pure Chemical Industries, Ltd. D-Glucose was purchased from Junsei Chemical Co. Ltd. $H_2PtCl_6 \cdot 6H_2O$ and Pt/C (TEC10V30E) was purchased from Tanaka Kikinzoku Kogyo. Polybenzimidazole (PBI) fine powder was purchased from Sato Light Industrial Co., Ltd. Vertically aligned carbon nanotube (VACNT, ZEONANO^{TM} SG101) was provided by ZEON Co., Ltd.

Preparation of Pt–Ni rhombic dodecahedral nanoframes. Pt–Ni rhombic dodecahedral nanoframes (NFs) were prepared based on the synthetic procedure reported.[8,29-30]

$H_2PtCl_6 \cdot 6H_2O$ (100 mg, 0.193 mmol), $Ni(NO_3)_2 \cdot 6H_2O$ (87.5 mg, 0.301 mmol) and oleylamine (50 mL, 0.152 mol) were mixed in a two-necked flask (100 mL). The reaction mixture was heated in an oil bath at 443 K under Ar for approximately 1 h, heated in an aluminum block at 543 K under Ar for ca. 20 min to obtain the slurry in black, and then further heated for ca. 4 min. Following heating, the reaction flask was put in an ice bath to quench the reaction. A Pt−Ni bimetallic precursor was isolated from the reaction mixture at 10,000 rpm for 10 min at each step using a Micro Refrigerated Centrifuge 3700 equipped with an angle rotor AF-5004CA (Kubota Co.) and then rinsed with the ethanol and hexane mixture (ca. 20 mL, 1:1 v/v) under centrifugation at 10,000 rpm for 10 min at least 8 times to obtain the rhombic dodecahedral precursor. Yield: ca. 10 mg.

The isolated precursor was dispersed in a mixture of oleylamine (1 mL), acetic acid (20 mL), toluene (20 mL) in an eggplant-shaped flask (100 mL), and then the reaction mixture was refluxed in an oil bath at 363 K for 2 h in air. The product was isolated from the reaction mixture

and rinsed with the ethanol and hexane mixture (ca. 20 mL, 1:1 v/v) under centrifugation at 10,000 rpm for 10 min at least 8 times to obtain NF. The obtained NFs were stored in ethanol in a dark environment to prevent aggregation. Yield: ca. 7 mg.

Preparation of nitrogen-doped carbon support. Nitrogen-doped carbon (NC) was prepared based on the reported procedure.[8] Melamine (15 g, 0.12 mol) and D-glucose (0.75 g, 4.2 mmol) were ground uniformly with a mortar and a pestle, placed in an alumina crucible covered with a lid, heated in a furnace (FP22, Yamato Scientific Co., LTD.) at 823 K for 3 h in air, and then cooled to room temperature in the furnace. The heated sample (ca. 2.5 g) was placed in a quartz boat and then transferred into a quartz tube (I.D.: 26 mm; O.D.: 30 mm; length: 450 mm) for heating in a tube furnace (ARF-30KC, Asahi-rika) that was equipped with a temperature controller (AGC-N, Asahi-rika). The sample was pre-heated at 373 K for 1 h under an argon flow of 200 sccm, and then heated at 1223 K for 3 h under an argon flow at 200 sccm. After the heat treatment, the sample in the quartz tube was cooled using an electric fan to room temperature. Yield: ca. 40 mg.

Preparation of PBI/VACNT composite. A PBI/VACNT composite was prepared based on synthetic procedures previously reported.[22-23] VACNT (5.0 mg) were added into a DMAc (5 mL) solution containing PBI fine powder (20 mg), dispersed under ultrasonication in an ultrasonic bath (AU-80C, Aiwa Ika Kougyo) for 20 min, and then vortexed for 3 h using Vortex-Genie 2 (Scientific Industries, Inc.). The PBI/VACNT composite was collected under vacuum filtration, rinsed with DMAc to remove any unbound PBI, and then dried at 353 K under vacuum overnight. Yield: ca. 7 mg.

Preparation of NFs supported on Vulcan XC-72 (NF/C). Vulcan XC-72 (at least 1 mg) was dispersed in ethanol (ca. 10 mL) under ultrasonication. NFs were added into the dispersion, where the weight ratio of NFs to the support was maintained at 3:7, and then sonicated in an ice-water mixture in the ultrasonic bath for 1 h. The solvent was removed using a Smart Evaporator (C1, BioChromato) and then the product was dried in the furnace at 473 K for 12 h in air to remove organic contaminants.

Preparation of NFs supported on NC (NF/NC). NC (at least 1 mg) was dispersed in ethanol under ultrasonication using an ultrasonic homogenizer (Branson Analog Sonifier 250A) with the minimum power output for several minutes. NFs were added into the dispersion, where the weight ratio of NFs to the support was maintained at 3:7, and then sonicated in an ice-water mixture in the ultrasonic bath for 1 h. The solvent was removed using the Smart Evaporator and then dried in the furnace at 473 K for 12 h in air.

Preparation of NFs supported on VACNT or PBI/VACNT (NF/VACNT and NF/PBI/VACNT). VACNT or PBI/VACNT (at least 1 mg) was dispersed in DMAc (ca. 10 mL) under ultrasonication using the ultrasonic homogenizer with 20 W (duty cycle: 50%) for 10 min. NFs were added into the dispersion, where the weight ratio of NFs to the support was maintained at 3:7, and then sonicated in an ice-water mixture in the ultrasonic bath for 1 h. The products of NF/VACNT and NF/PBI/VACNT were kept in solution due to their low dispersibility in solution after completely drying them.

Electrochemical measurements. Electrochemical measurements were performed using a conventional three-electrode setup. A potentiostat (HZ-7000, Hokuto Denko) was used to perform cyclic voltammetry (CV) and linear sweep voltammetry (LSV). A rotating disk

electrode (RDE) was used as the working electrode. An Ag|AgCl (sat. KCl) electrode with a double junction holder (International chemistry Co., Ltd) and platinum foil were used as the reference electrode and the counter electrode, respectively. Catalyst-modified glassy carbon (GC) was used as the working electrode.

A GC screw (5 mm φ, M4, Tokai Carbon Co., Ltd.) or a GC disk (5 mm φ, Tokai Carbon Co., Ltd.) was polished with alumina slurry (0.3 μm, Baikalox), followed by alumina slurry (0.05 μm, Baikalox), and then sonicated in acetone and Milli-Q water for at least 5 min each before drop-casting a catalytic ink. To prepare the catalyst ink, 0.70 mg of each catalyst (NF/C, NF/NC, NF/VACNT, NF/PBI/VACNT or Pt/C) was dispersed in a mixture of 0.30 mL of 2-propanol, 0.95 mL of Milli-Q water and 5.0 μL of 5% Nafion DE520 in an ice–water mixture under ultrasonication. The NF/C ink and NF/NC ink was kept under ultrasonication for 2 h using the ultrasonic bath, whereas the ultrasonic homogenizer was used for the NF/VACNT and NF/PBI–VACNT ink for 4 min. For all catalysts except for NF/VACNT, the catalyst ink (15–20 μL) was drop-cast on the GC disk that was rotating at 700 rpm using an AFMSRX Analytical Rotator and a MSRX Speed Controller (PINE Research Instrumentation) and then dried at room temperature. In the case of NF/VACNT, the ink was drop-cast on the GC disk and then immediately heated at 373 K for 5 min in a furnace (FP22, Yamato Scientific). For *in situ* XAFS measurements, the catalyst-modified GC screws were heated at 418 K for 5 min.

CVs and LSVs were recorded in an aqueous solution containing 0.1 M $HClO_4$. The electrolyte solution was purged with argon or oxygen for at least 30 min before electrochemical measurements. All LSVs undergoing positive sweep under oxygen are corrected by the subtraction of the current densities of the corresponding working electrode recorded under Ar. All potentials are shown against the RHE.

For CO stripping measurements, a 0.1 M $HClO_4$ aqueous electrolyte solution was purged with CO for 5 min and then with Ar for 60 min. A bias potential of 0.05 V vs. RHE was applied to a sample electrode during purging with CO and Ar until the measurements began. Cyclic voltammograms were recorded in the potential range from 0.05 to 1.45 V vs. RHE for two cycles. Electrochemically active surface areas based on electrochemical oxidation of CO charges were determined from the difference between the first and second cycles.

Physicochemical measurements. X-ray photoelectron spectroscopy (XPS) data were collected at a pass energy of 10 eV using an Al Kα X-ray source on a photoelectron spectrometer JPS-9200 (JEOL). The C=C peak in the C1s region was used as the internal standard (284.6 eV). A catalyst ink was drop-cast onto a glassy carbon plate (ca. 1x1 cm^2) at 343 K and then dried under vacuum overnight. Elemental analysis on PBI/VACNT was done using a CHN Analyzer (JM10, J-SCIENCE LAB Co., Ltd.) at the Global Facility Center, Hokkaido University, Japan. Inductively coupled plasma atomic emission spectroscopy (ICP–AES) was performed using an ICP–AES spectrometer ICPE-9000 (Shimazu Corp.). For sample preparation, a catalyst ink was dispersed in aqua regia solution and then the dispersion was stirred at 308 K for 48 h. The dispersion was filtered through a membrane filter (13HP045AN, ADVANTEC), and then the filtrate was diluted with Milli-Q water. STEM images were taken at an acceleration voltage of 200 kV using HD-2000 (Hitach Scientific Instrument). HAADF–STEM and EDS elemental mapping images were taken using a JEOL JEM-ARM200F instrument at 200 kV.

***In situ* XAS measurements.** In situ Pt L_{III}-edge XAS data at the RDE in 0.1 M $HClO_4$ under nitrogen were collected using a 21 Ge-element detector in a fluorescent method at BL36XU station in SPring-8.[36] XANES spectra were normalized using Athena software.[37] Catalyst-modified GC, platinum foil and reversible hydrogen (International chemistry Co., Ltd) electrodes

were used as the working, counter and reference electrodes, respectively. Electrochemical data were collected using AutoLab Potential and Galvanostat system (Metrohm). Before *in situ* XAS measurements, 0.1 M $HClO_4$ aqueous electrolyte solution in a polyether ether ketone (PEEK) cell was purged with nitrogen for at least 30 min and then 50 potential cycles at 200 mV s^{-1} were performed in the potential range from 0.05 to 1.0 V vs. RHE under nitrogen for electrochemical cleaning. XANES spectra of the catalysts were obtained at 0.4, 0.7, 0.9, 1.0 and 1.1 V vs. RHE under nitrogen.

RESULTS AND DISCUSSION

NFs were prepared based on the reported procedures in two steps: preparation of a Pt–Ni rhombic dodecahedral precursor in the first step and chemical corrosion of it to the NF in the second step.[8,29-30] The key to the preparation of NFs is a heating period in the first step: heating an oleylamine solution containing $H_2PtCl_6 \cdot 6H_2O$ and $Ni(NO_3)_2 \cdot 6H_2O$ at 543 K under Ar gave rhombic dodecahedron nanocrystals that have Pt-enriched corners and edges. Less-heating gave a highly branched, Pt-rich tetradecapod structure embedded in a Ni-rich shell,[38-39] whereas over-heating produced a tetradecapod structure in a Pt-rich shell (**Figures S1** and **S2**). In the second step, the rhombic dodecahedron nanocrystals can be converted to NFs in the solvent mixture of oleylamine, acetic acid and toluene at 363 K for 2 h under the air, but the others did not.

Next, NFs were immobilized on each support (**Figure 1a**). VACNTs were wrapped with PBI in dimehylacetamide under ultrasonication.[22-23] NC was prepared from melamine and glucose in the reported procedure.[8,40] Elemental analysis of NC and PBI/VACNT gave nitrogen contents of 9 and 6 wt%, respectively. Changing different mixing ratios of PBI and VACNT gave almost the same nitrogen content, indicating that the washing treatment removed excess amounts of PBI

from the VACNT surface and then gave a uniform film of PBI on VACNTs.[22-23] STEM images of VACNT and PBI/VACNT images before and after NF immobilization are shown in **Figures 1b–1e**. NFs were immobilized on either PBI-coated or uncoated VACNTs. It seems that PBI-coating unbundled VACNTs and NFs were homogeneously placed on PBI/VACNT whereas NFs were aggregated on bundled VACNTs in the absence of PBI. The PBI-wrapping also provides nitrogen donor sites, which interact with the surface Pt of NFs, resulting in the highly dispersed immobilization of NFs on PBI-coated VACNTs.

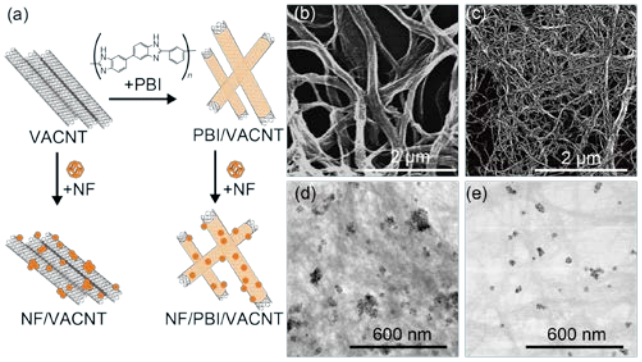

Figure 1. (a) Scheme of synthesis of NF/VACNT and NF/PBI/VACNT. STEM images of (b) VACNT, (c) PBI/VACNT, (d) NF/VACNT and (e) NF/PBI/VACNT.

The PBI-coating of VACNTs improved the ORR activity of NFs, confirmed by recording linear sweep voltammograms (LSVs) using rotating disk electrodes in 0.1 M $HClO_4$ aq. under O_2 (**Figure 2a**). Both of NF/PBI/VACNT and NF/VACNT showed negative currents when involving the ORR. A half wave potential ($E_{1/2}$) of NF/PBI/VACNT was +0.90 V vs. RHE, which was more positive than that of NF/VACNT (+0.82 V vs. RHE). Mass and specific activities of NF/PBI/VACNT were determined to be 1.3×10^2 A g_{Pt}^{-1} and 3.6 A m_{Pt}^{-2} at +0.95 V vs. RHE, respectively (**Table S1**). These values are slightly larger than those of NF/VACNT (1.1

$\times 10^2$ A g_{Pt}^{-1} and 2.2 A m_{Pt}^{-2} at +0.95 V vs. RHE). NF/PBI/VACNT seems to show slightly higher ORR activity than NF/VACNT, but much lower than NF/NC (3.5×10^2 A g_{Pt}^{-1} and 5.6 A m_{Pt}^{-2} at +0.95 V vs. RHE), which is already known to show higher activity than than NF/C (**Figure 2b**).[8] One of the possible explanations on the activity difference between NF/PBI/VACNT and NF/NC may come from the difference in electrical resistivity: PBI is a semiconductor with a high electrical resistivity of $>10^{12}$ Ω cm;[41] NC is conductive ($>10^1$ Ω cm).[8,40] The electrical resistivity of supports is known to affect the catalytic activity of Pt-based catalysts immobilized.[8,16,21] NFs immobilized on more conductive NC supports could show higher activity than those on less conductive PBI-coated VACNTs.

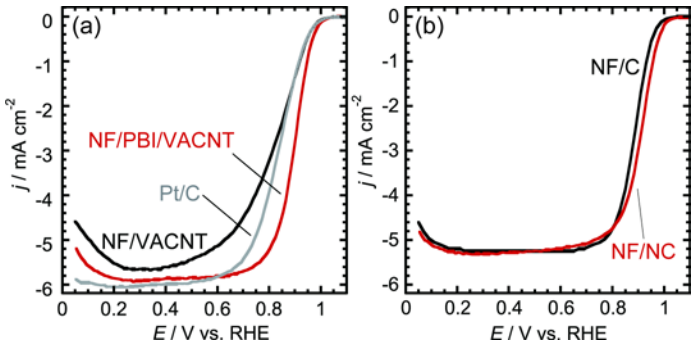

Figure 2. (a) LSVs of NF/VACNT (in black), NF/PBI/VACNT (in red) and Pt/C (in gray) and (b) LSVs of NF/C (in black) and NF/NC (in red) at 10 mV s^{-1} in 0.1 M $HClO_4$ aqueous solution under O_2 at 1600 rpm.

To understand electronic effects of PBI-wrapping on the surface Pt of NFs, *ex situ* XPS of NF/VACNT and NF/PBI/VACNT was performed in the Pt 4f region (**Figure S3**). Peak deconvolution analysis revealed the presence of Pt^0 and Pt^{II} components. However, there is

almost no significant peak shift of each component for NF/PBI/VACNT, compared with those of NF/VACNT (**Table S2**). Almost no difference of Pt^0/Pt^{II} ratios was also confirmed between NF/PBI/VACNT and NF/VACNT. Previously, positive peak shifts were reported for Pt nanoparticles supported on NC (+0.2–0.3 eV), compared to non-doped carbon supports.[7,13-16] Similar positive peak shifts were also observed for NF/NC.[8] Because such a binding energy shift indicates an interaction between nitrogen atoms of supports and the surface Pt of NFs, PBI-coated supports gave almost no impact on the electronic state of the surface Pt of NFs but NC supports did.

To clarify the difference in electronic effects on the catalytic activity between PBI-coating and N-doping approaches, we performed *in situ* Pt L_{III}-edge XAS of NF/PBI/VACNT, NF/VACNT, NF/C and NF/NC in 0.1 M $HClO_4$ under Ar under potential control (**Figure 3**). In Pt L_{III}-edge X-ray absorption near-edge structure (XANES) region, white line peak intensities are known to be sensitive to changes in the oxidation state of Pt because the white line peak ($2p \rightarrow 5d$ transition) intensity reflects the degree of the vacancy of Pt 5d orbitals near the Fermi level.[36] In other words, higher intensities means higher oxidation states of Pt. Plots of white line peak intensities against potential show a clear difference between NF/C and NF/NC: the peak intensity depended on potential and there was a hysteresis for NF/C but not for NF/NC (**Figure 3c**). This result indicates that the formation of oxygenated Pt species such as $Pt(OH)_{ad}$ is clearly suppressed in the case of NF/NC.[27,42-44] This is because of the downshift of the d-band center position of the surface Pt.[8] In contrast, almost no difference was observed between NF/PBI/VACNT and NF/VACNT (**Figure 3f**), even though these catalysts showed different catalytic activity as mentioned above. This is because coating Pt nanoparticles with nitrogen-

containing polymers increases the rate of formation of $Pt(OH)_{ad}$ species *via* hydrogen bonding with nitrogen atoms.[45-46]

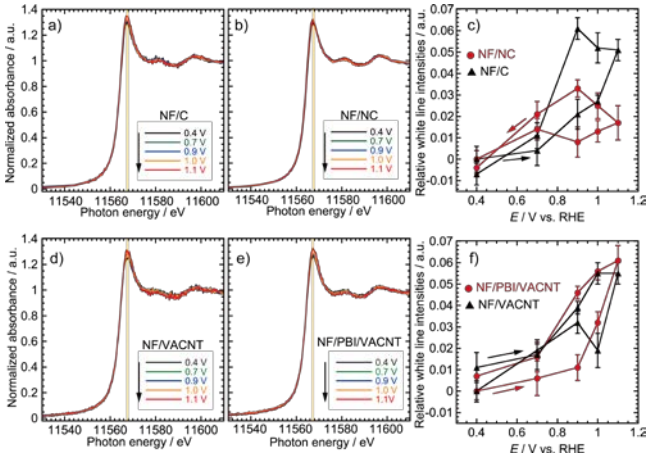

Figure 3. Potential dependent XANES spectra of (a) NF/C and (b) NF/NC and (c) plots of relative white line peak intensities of NF/C and NF/NC against potential. Potential dependent XANES spectra of (d) NF/ VACNT, (e) NF/PBI/VACNT and (f) plots of relative white line peak intensities of NF/VACNT and NF/PBI/VACNT against potential. Potentials were applied stepwise from +0.4 to +1.1 and +0.4 V vs. RHE in 0.1 M $HClO_4$ aq. under nitrogen. Averaged data points ranging from 11567 to 11568 eV in photon energy were plotted as white line peak intensities in (c) and (f). Enlarged XANES spectra in the white line region are available in **Figure S4**.

To gain more insights into the difference between nitrogen-doping and PBI-wrapping approaches, electrochemical CO stripping experiments were performed for NF/PBI/VACNT and NF/VACNT. Electrochemical CO stripping measurements are sensitive to the surface composition and defect density, and CO stripping peak potentials are directly correlated with the

Pt d-band center.[47-48] Although a clear negative potential shift of ca. 0.1 V was previously observed for NF/NC, compared with NF/C,[8] such an obvious potential shift was not observed between NF/PBI/VACNT and NF/VACNT (**Figure 4**). This result is in good agreement with the results in XPS and XAS. Interestingly, the oxidation wave for NF/PBI/VACNT was wider than that of NF/VACNT. This broadening possibly originates from the interaction of CO_{ad} species with $Pt(OH)_{ad}$ species that can be stabilized with PBI.[45-46,49] Thus, the activity improvement in the PBI-coating method derives from a factor other than electronic effects at the catalyst/support interface: proton accessibility to the Pt surface induced by the formation of a uniform Nafion film.[22]

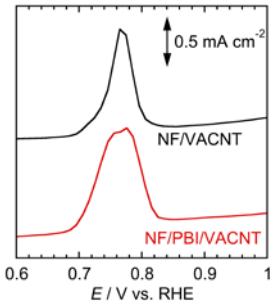

Figure 4. Electrochemical CO stripping voltammograms of NF/PBI/VACNT (in red) and NF/VACNT (in black) at 50 mV s^{-1} in 0.1 M $HClO_4$ aqueous solution under Ar.

CONCLUSIONS

We revealed the difference in catalytic and electronic behaviour between Pt_3Ni NFs immobilized on PBI-coated/uncoated VACNTs. Although PBI-coated VACNTs improved the catalytic

activity of immobilized NFs, *ex situ* XPS and *in situ* XAS measurements demonstrated that PBI-coated VACNTs showed no clear electronic effect on NFs, unlike the N-doped carbon support. The PBI-coating approach keeps the electronic state of nanostructured Pt-alloy electrocatalysts immobilized on supports almost intact but stabilizes $Pt(OH)_{ad}$ species under electrochemical conditions, leading to the enhancement of the catalytic activity of the catalyst immobilized. Compared with N-doping approaches, polymer-coating approaches have greater advantages such as simple synthetic procedures and non-destructive, uniform modification of carbon supports. These advantages would allow us to improve the dispersibility of carbon supports and catalysts, proton conductivity, the stability of supports and Pt utilization efficiency. Polymer-coating approaches would open up new possibilities of maximizing the activity and durability of Pt-alloy nanostructured electrocatalysts with almost no electronic effect.

ASSOCIATED CONTENT

Supporting Information.

The following files are available free of charge.

Schematic representation of the growth mechanism of the rhombic dodecahedron and NFs

TEM images of the precursors

X-ray photoelectron spectra and enlarged potential dependent XANES spectra (PDF)

AUTHOR INFORMATION

Corresponding Author

*masaru.kato@ees.hokudai.ac.jp(MK);

iyagi@ees.hokudai.ac.jp (IY)

ACKNOWLEDGMENTS

The authors thank Shingo Mukai, Yusuke Kawamura (Technical Division, Institute for Catalysis, Hokkaido University) and Takao Ohta (Graduate School of Engineering, Hokkaido University) for their technical support on electrochemical setups; Naomi Hirai (Research Institute for Electronic Science, Hokkaido University) for taking the HAADF–STEM and EDS mapping images; and Dr. Tomohiro Sakata and Prof. Yasuhiro Iwasawa (The University of Electro-Communications) for fruitful discussion on XAS measurements.

This work was supported by the project “Development of Advanced PEFC Utilization Technologies/Development of Fundamental Technologies for PEFC Promotion/Highly-Coupled Analysis of Phenomena in MEA and its Constituents and Evaluation of Cell Performance” of NEDO, Japan and "Nanotechnology Platform" Program of the Ministry of Education, Culture,

Sports, Science and Technology (MEXT) for Hokkaido University. XAS was performed at the beamline BL36XU, SPring-8, Japan (Proposal Nos. 2018A7903, 2019A7903 and 2019B7903).

REFERENCES

(1) Gerber, I. C.; Serp, P. A Theory/Experience Description of Support Effects in Carbon-Supported Catalysts. *Chem. Rev.* **2020,** *120* (2), 1250-1349, DOI: 10.1021/acs.chemrev.9b00209.
(2) Campisi, S.; Chan-Thaw, C. E.; Villa, A. Understanding Heteroatom-Mediated Metal-Support Interactions in Functionalized Carbons: A Perspective Review. *Appl. Sci.* **2018,** *8* (7), DOI: 10.3390/app8071159.
(3) He, Z.; Dong, B.; Wang, W.; Yang, G.; Cao, Y.; Wang, H.; Yang, Y.; Wang, Q.; Peng, F.; Yu, H. Elucidating Interaction between Palladium and N-Doped Carbon Nanotubes: Effect of Electronic Property on Activity for Nitrobenzene Hydrogenation. *ACS Catal.* **2019,** *9* (4), 2893-2901, DOI: 10.1021/acscatal.8b03965.
(4) Jin, Y.; Zhao, J.; Li, F.; Jia, W.; Liang, D.; Chen, H.; Li, R.; Hu, J.; Ni, J.; Wu, T.; Zhong, D. Nitrogen-doped graphene supported palladium-nickel nanoparticles with enhanced catalytic performance for formic acid oxidation. *Electrochim. Acta* **2016,** *220*, 83-90, DOI: https://doi.org/10.1016/j.electacta.2016.10.087.
(5) Ott, S.; Orfanidi, A.; Schmies, H.; Anke, B.; Nong, H. N.; Hübner, J.; Gernert, U.; Gliech, M.; Lerch, M.; Strasser, P. Ionomer distribution control in porous carbon-supported catalyst layers for high-power and low Pt-loaded proton exchange membrane fuel cells. *Nat. Mater.* **2020,** *19* (1), 77-85, DOI: 10.1038/s41563-019-0487-0.
(6) Karuppannan, M.; Kim, Y.; Gok, S.; Lee, E.; Hwang, J. Y.; Jang, J.-H.; Cho, Y.-H.; Lim, T.; Sung, Y.-E.; Kwon, O. J. A highly durable carbon-nanofiber-supported Pt–C core–shell cathode catalyst for ultra-low Pt loading proton exchange membrane fuel cells: facile carbon encapsulation. *Energy Environ. Sci.* **2019,** *12* (9), 2820-2829, DOI: 10.1039/C9EE01000A.
(7) Zhang, S.; Fu, T.; Li, J.; Peng, Y.; Zhao, J. Platinum Nanoparticles Dispersed on High-Surface-Area Roelike Nitrogen-Doped Mesoporous Carbon for Oxygen Reduction Reaction. *ACS Appl. Energy Mater*. **2018,** *1* (11), 6198-6207, DOI: 10.1021/acsaem.8b01242.
(8) Kato, M.; Ogura, K.; Nakagawa, S.; Tokuda, S.; Takahashi, K.; Nakamura, T.; Yagi, I. Enhancement of Electrocatalytic Oxygen Reduction Activity and Durability of Pt–Ni Rhombic Dodecahedral Nanoframes by Anchoring to Nitrogen-Doped Carbon Support. *ACS Omega* **2018,** *3* (8), 9052-9059, DOI: 10.1021/acsomega.8b01373.
(9) Brandiele, R.; Durante, C.; Zerbetto, M.; Vicentini, N.; Kosmala, T.; Badocco, D.; Pastore, P.; Rizzi, G. A.; Isse, A. A.; Gennaro, A. Probing the correlation between Pt-support interaction and oxygen reduction reaction activity in mesoporous carbon materials modified with Pt-N active sites. *Electrochim. Acta* **2018,** *277*, 287-300, DOI: https://doi.org/10.1016/j.electacta.2018.04.182.
(10) Kabir, S.; Serov, A.; Artyushkova, K.; Atanassov, P. Nitrogen-Doped Three-Dimensional Graphene-Supported Palladium Nanocomposites: High-Performance Cathode Catalysts for Oxygen Reduction Reactions. *ACS Catal.* **2017,** *7* (10), 6609-6618, DOI: 10.1021/acscatal.7b02071.
(11) Sun, L.; Liao, B.; Ren, X.; Li, Y.; Zhang, P.; Deng, L.; Gao, Y. Ternary PdNi-based nanocrystals supported on nitrogen-doped reduced graphene oxide as highly active

electrocatalysts for the oxygen reduction reaction. *Electrochim. Acta* **2017,** *235*, 543-552, DOI: https://doi.org/10.1016/j.electacta.2017.03.159.
(12) Wang, J.; Liu, L.; Chou, S.; Liu, H.; Wang, J. A 3D porous nitrogen-doped carbon-nanofiber-supported palladium composite as an efficient catalytic cathode for lithium–oxygen batteries. *J. Mater. Chem. A* **2017,** *5* (4), 1462-1471, DOI: 10.1039/C6TA07050G.
(13) Perini, L.; Durante, C.; Favaro, M.; Perazzolo, V.; Agnoli, S.; Schneider, O.; Granozzi, G.; Gennaro, A. Metal–Support Interaction in Platinum and Palladium Nanoparticles Loaded on Nitrogen-Doped Mesoporous Carbon for Oxygen Reduction Reaction. *ACS Appl. Mater. Interf.* **2015,** *7* (2), 1170-1179, DOI: 10.1021/am506916y.
(14) Perazzolo, V.; Brandiele, R.; Durante, C.; Zerbetto, M.; Causin, V.; Rizzi, G. A.; Cerri, I.; Granozzi, G.; Gennaro, A. Density Functional Theory (DFT) and Experimental Evidences of Metal–Support Interaction in Platinum Nanoparticles Supported on Nitrogen- and Sulfur-Doped Mesoporous Carbons: Synthesis, Activity, and Stability. *ACS Catal.* **2018,** *8* (2), 1122-1137, DOI: 10.1021/acscatal.7b03942.
(15) Nie, Y.; Deng, J.; Chen, S.; Wei, Z. Promoting stability and activity of PtNi/C for oxygen reduction reaction via polyaniline-confined space annealing strategy. *Int. J. Hydrog. Energy* **2019,** *44* (12), 5921-5928, DOI: 10.1016/j.ijhydene.2019.01.125.
(16) Cao, J. Y.; Hu, Y.; Chen, L. J.; Xu, J.; Chen, Z. D. Nitrogen-doped carbon quantum dot/graphene hybrid nanocomposite as an efficient catalyst support for the oxygen reduction reaction. *Int. J. Hydrog. Energy* **2017,** *42* (5), 2931-2942, DOI: 10.1016/j.ijhydene.2017.01.029.
(17) Wang, Q.; Tian, Y.; Chen, G. J.; Zhao, J. X. Theoretical insights into the energetics and electronic properties of MPt12 (M = Fe, Co, Ni, Cu, and Pd) nanoparticles supported by N-doped defective graphene. *Appl. Surf. Sci.* **2017,** *397*, 199-205, DOI: 10.1016/j.apsusc.2016.11.048.
(18) Ichihashi, K.; Muratsugu, S.; Miyamoto, S.; Sakamoto, K.; Ishiguro, N.; Tada, M. Enhanced oxygen reduction reaction performance of size-controlled Pt nanoparticles on polypyrrole-functionalized carbon nanotubes. *Dalton Trans.* **2019,** *48* (21), 7130-7137, DOI: 10.1039/C9DT00158A.
(19) Melke, J.; Peter, B.; Habereder, A.; Ziegler, J.; Fasel, C.; Nefedov, A.; Sezen, H.; Wöll, C.; Ehrenberg, H.; Roth, C. Metal–Support Interactions of Platinum Nanoparticles Decorated N-Doped Carbon Nanofibers for the Oxygen Reduction Reaction. *ACS Appl. Mater. Interf.* **2016,** *8* (1), 82-90, DOI: 10.1021/acsami.5b06225.
(20) Chen, S.; Wei, Z.; Qi, X.; Dong, L.; Guo, Y.-G.; Wan, L.; Shao, Z.; Li, L. Nanostructured Polyaniline-Decorated Pt/C@PANI Core–Shell Catalyst with Enhanced Durability and Activity. *J. Am. Chem. Soc.* **2012,** *134* (32), 13252-13255, DOI: 10.1021/ja306501x.
(21) Li, L.; Hu, L. P.; Li, J.; Wei, Z. D. Enhanced stability of Pt nanoparticle electrocatalysts for fuel cells. *Nano Res* **2015,** *8* (2), 418-440, DOI: 10.1007/s12274-014-0695-5.
(22) Jayawickrama, S. M.; Han, Z. Y.; Kido, S.; Nakashima, N.; Fujigaya, T. Enhanced platinum utilization efficiency of polymer-coated carbon black as an electrocatalyst in polymer electrolyte membrane fuel cells. *Electrochim. Acta* **2019,** *312*, 349-357, DOI: 10.1016/j.electacta.2019.05.007.
(23) Okamoto, M.; Fujigaya, T.; Nakashima, N. Design of an Assembly of Poly(benzimidazole), Carbon Nanotubes, and Pt Nanoparticles for a Fuel-Cell Electrocatalyst with an Ideal Interfacial Nanostructure. *Small* **2009,** *5* (6), 735-740, DOI: 10.1002/smll.200801742.
(24) Yang, Z.; Li, J.; Ling, Y.; Zhang, Q.; Yu, X.; Cai, W. Bottom-up Design of High-Performance Pt Electrocatalysts Supported on Carbon Nanotubes with Homogeneous Ionomer Distribution. *ChemCatChem* **2017,** *9* (17), 3307-3313, DOI: 10.1002/cctc.201700587.

(25) Ahn, S. M.; Jeong, H. Y.; Jang, J.-K.; Lee, J. Y.; So, S.; Kim, Y. J.; Hong, Y. T.; Kim, T.-H. Polybenzimidazole/Nafion hybrid membrane with improved chemical stability for vanadium redox flow battery application. *RSC Adv.* **2018,** *8* (45), 25304-25312, DOI: 10.1039/C8RA03921F.
(26) Yang, Z.; Fujigaya, T.; Nakashima, N. Homogeneous coating of ionomer on electrocatalyst assisted by polybenzimidazole as an adhesive layer and its effect on fuel cell performance. *J. Power Sources* **2015,** *300*, 175-181, DOI: 10.1016/j.jpowsour.2015.09.069.
(27) Stamenkovic, V. R.; Fowler, B.; Mun, B. S.; Wang, G. F.; Ross, P. N.; Lucas, C. A.; Markovic, N. M. Improved oxygen reduction activity on Pt3Ni(111) via increased surface site availability. *Science* **2007,** *315* (5811), 493-497, DOI: 10.1126/science.1135941.
(28) Stamenkovic, V.; Mun, B. S.; Mayrhofer, K. J. J.; Ross, P. N.; Markovic, N. M.; Rossmeisl, J.; Greeley, J.; Nørskov, J. K. Changing the Activity of Electrocatalysts for Oxygen Reduction by Tuning the Surface Electronic Structure. *Angew. Chem. Int. Ed.* **2006,** *45* (18), 2897-2901, DOI: 10.1002/anie.200504386.
(29) Chen, C.; Kang, Y. J.; Huo, Z. Y.; Zhu, Z. W.; Huang, W. Y.; Xin, H. L. L.; Snyder, J. D.; Li, D. G.; Herron, J. A.; Mavrikakis, M.; Chi, M. F.; More, K. L.; Li, Y. D.; Markovic, N. M.; Somorjai, G. A.; Yang, P. D.; Stamenkovic, V. R. Highly Crystalline Multimetallic Nanoframes with Three-Dimensional Electrocatalytic Surfaces. *Science* **2014,** *343* (6177), 1339-1343, DOI: 10.1126/science.1249061.
(30) Chen, S. P.; Niu, Z. Q.; Xie, C. L.; Gao, M. Y.; Lai, M. L.; Li, M. F.; Yang, P. D. Effects of Catalyst Processing on the Activity and Stability of Pt-Ni Nanoframe Electrocatalysts. *ACS Nano* **2018,** *12* (8), 8697-8705, DOI: 10.1021/acsnano.8b04674.
(31) Stephens, I. E. L.; Rossmeisl, J.; Chorkendorff, I. Toward sustainable fuel cells. *Science* **2016,** *354* (6318), 1378-1379, DOI: 10.1126/science.aal3303.
(32) Yu, M.; Funke, H. H.; Falconer, J. L.; Noble, R. D. High Density, Vertically-Aligned Carbon Nanotube Membranes. *Nano Lett.* **2009,** *9* (1), 225-229, DOI: 10.1021/nl802816h.
(33) Futaba, D. N.; Hata, K.; Yamada, T.; Hiraoka, T.; Hayamizu, Y.; Kakudate, Y.; Tanaike, O.; Hatori, H.; Yumura, M.; Iijima, S. Shape-engineerable and highly densely packed single-walled carbon nanotubes and their application as super-capacitor electrodes. *Nat. Mater.* **2006,** *5* (12), 987-994, DOI: 10.1038/nmat1782.
(34) Yasuda, S.; Furuya, A.; Uchibori, Y.; Kim, J.; Murakoshi, K. Iron–Nitrogen-Doped Vertically Aligned Carbon Nanotube Electrocatalyst for the Oxygen Reduction Reaction. *Adv. Funct. Mater.* **2016,** *26* (5), 738-744, DOI: 10.1002/adfm.201503613.
(35) Yasuda, S.; Uchibori, Y.; Wakeshima, M.; Hinatsu, Y.; Ogawa, H.; Yano, M.; Asaoka, H. Enhancement of Fe–N–C carbon catalyst activity for the oxygen reduction reaction: effective increment of active sites by a short and repeated heating process. *RSC Adv.* **2018,** *8* (66), 37600-37605, DOI: 10.1039/C8RA08359B.
(36) Nagasawa, K.; Takao, S.; Nagamatsu, S.; Samjeske, G.; Sekizawa, O.; Kaneko, T.; Higashi, K.; Yamamoto, T.; Uruga, T.; Iwasawa, Y. Surface-Regulated Nano-SnO2/Pt3Co/C Cathode Catalysts for Polymer Electrolyte Fuel Cells Fabricated by a Selective Electrochemical Sn Deposition Method. *J. Am. Chem. Soc.* **2015,** *137* (40), 12856-12864, DOI: 10.1021/jacs.5b04256.
(37) Ravel, B.; Newville, M. ATHENA, ARTEMIS, HEPHAESTUS: data analysis for X-ray absorption spectroscopy using IFEFFIT. *J. Synchrotron Radiat.* **2005,** *12*, 537-541, DOI: 10.1107/S0909049505012719.

(38) Niu, Z. Q.; Becknell, N.; Yu, Y.; Kim, D.; Chen, C.; Kornienko, N.; Somorjai, G. A.; Yang, P. D. Anisotropic phase segregation and migration of Pt in nanocrystals en route to nanoframe catalysts. *Nat. Mater.* **2016,** *15* (11), 1188-1194, DOI: 10.1038/Nmat4724.
(39) Tan, S. F.; Chee, S. W.; Baraissov, Z.; Jin, H.; Tan, T. L.; Mirsaidov, U. Intermediate Structures of Pt–Ni Nanoparticles during Selective Chemical and Electrochemical Etching. *J. Phys. Chem. Lett.* **2019,** *10* (20), 6090-6096, DOI: 10.1021/acs.jpclett.9b02388.
(40) Zhang, Y. W.; Ge, J.; Wang, L.; Wang, D. H.; Ding, F.; Tao, X. M.; Chen, W. Manageable N-doped Graphene for High Performance Oxygen Reduction Reaction. *Sci. Rep.* **2013,** *3*, DOI: 10.1038/srep02771.
(41) Pohl, H. A.; Chartoff, R. P. Carriers and unpaired spins in some organic semiconductors. *J. Polymer Sci.* **1964,** *2* (6), 2787-2806, DOI: 10.1002/pol.1964.100020629.
(42) Lee, S. W.; Chen, S.; Suntivich, J.; Sasaki, K.; Adzic, R. R.; Shao-Horn, Y. Role of Surface Steps of Pt Nanoparticles on the Electrochemical Activity for Oxygen Reduction. *J. Phys. Chem. Lett.* **2010,** *1* (9), 1316-1320, DOI: 10.1021/jz100241j.
(43) Zhao, X.; Takao, S.; Higashi, K.; Kaneko, T.; Samjeske, G.; Sekizawa, O.; Sakata, T.; Yoshida, Y.; Uruga, T.; Iwasawa, Y. Simultaneous Improvements in Performance and Durability of an Octahedral PtNix/C Electrocatalyst for Next-Generation Fuel Cells by Continuous, Compressive, and Concave Pt Skin Layers. *ACS Catal.* **2017,** *7* (7), 4642-4654, DOI: 10.1021/acscatal.7b00964.
(44) Tian, X.; Zhao, X.; Su, Y.-Q.; Wang, L.; Wang, H.; Dang, D.; Chi, B.; Liu, H.; Hensen, E. J. M.; Lou, X. W.; Xia, B. Y. Engineering bunched Pt-Ni alloy nanocages for efficient oxygen reduction in practical fuel cells. *Science* **2019,** *366* (6467), 850-856, DOI: 10.1126/science.aaw7493.
(45) Fujigaya, T.; Okamoto, M.; Matsumoto, K.; Kaneko, K.; Nakashima, N. Interfacial Engineering of Platinum Catalysts for Fuel Cells: Methanol Oxidation is Dramatically Improved by Polymer Coating on a Platinum Catalyst. *ChemCatChem* **2013,** *5* (7), 1701-1704, DOI: 10.1002/cctc.201300157.
(46) Gharibi, H.; Amani, M.; Pahlavanzadeh, H.; Kazemeini, M. Investigation of carbon monoxide tolerance of platinum nanoparticles in the presence of optimum ratio of doped polyaniline with para toluene sulfonic acid and their utilization in a real passive direct methanol fuel cell. *Electrochim. Acta* **2013,** *97*, 216-225, DOI: 10.1016/j.electacta.2013.01.121.
(47) Jiang, T.; Mowbray, D. J.; Dobrin, S.; Falsig, H.; Hvolbæk, B.; Bligaard, T.; Nørskov, J. K. Trends in CO Oxidation Rates for Metal Nanoparticles and Close-Packed, Stepped, and Kinked Surfaces. *J. Phys. Chem. C* **2009,** *113* (24), 10548-10553, DOI: 10.1021/jp811185g.
(48) Hammer, B.; Nielsen, O. H.; Nrskov, J. K. Structure sensitivity in adsorption: CO interaction with stepped and reconstructed Pt surfaces. *Catal. Lett.* **1997,** *46* (1), 31-35, DOI: 10.1023/A:1019073208575.
(49) Sun, J.; Ling, Y.; Zhang, Q.; Yu, X.; Yang, Z. Simultaneous enhancements in stability and CO tolerance of Pt electrocatalyst by double poly(vinyl pyrrolidone) coatings. *RSC Adv.* **2017,** *7* (47), 29839-29843, DOI: 10.1039/C7RA04691J.

SYNOPSIS.